This document is the accepted manuscript version of the following article:

Grinenko, V., Ghosh, S., Sarkar, R., Orain, J. C., Nikitin, A., Elender, M., … Klauss, H. H. (2021). Split superconducting and time-reversal symmetry-breaking transitions in Sr2RuO4 under stress. Nature Physics. https://doi.org/10.1038/s41567-021-01182-7

SPLIT SUPERCONDUCTING AND TIME-REVERSAL SYMMETRY-BREAKING TRANSITIONS IN Sr_2RuO_4 UNDER STRESS

Vadim Grinenko[1,2,*,†], Shreenanda Ghosh,[1,*], Rajib Sarkar,[1], Jean-Christophe Orain[3], Artem Nikitin[3], Matthias Elender[3], Debarchan Das[3], Zurab Guguchia[3], Felix Brückner[1], Mark E. Barber,[4], Joonbum Park[4], Naoki Kikugawa[5], Dmitry A. Sokolov[4], Jake S. Bobowski[6,7], Takuto Miyoshi[6], Yoshiteru Maeno[6], Andrew P. Mackenzie[4,8], Hubertus Luetkens[3], Clifford W. Hicks[4,9,†], AND Hans-Henning Klauss[1,†]

1. Institute for Solid State and Materials Physics, Technische Universität Dresden

2. Leibniz IFW Dresden, D-01069, Dresden, Germany

3. Laboratory for Muon Spin Spectroscopy, PSI, CH-5232 Villigen PSI, Switzerland

4. Max Planck Institute for Chemical Physics of Solids, D-01187 Dresden, Germany

5. National Institute for Materials Science, Tsukuba 305-0003, Japan

6. Department of Physics, Kyoto University, Kyoto 606-8502, Japan

7. Physics, University of British Columbia, Kelowna, BC V1V 1V7, Canada

8. Scottish Universities Physics Alliance (SUPA), School of Physics and Astronomy, University of St. Andrews, St. Andrews KY16 9SS, United Kingdom

9. School of Physics and Astronomy, University of Birmingham, Birmingham B15 2TT, United Kingdom

*These authors contributed equally to this work

†Corresponding author. E-mail: vadim.a.grinenko@gmail.com (V.G.), C.Hicks.1@bham.ac.uk (C.W.H.), henning.klauss@tu-dresden.de (H.-H.K.)

Sr_2RuO_4 continues to present an important test of our understanding of unconventional superconductivity, because while its normal-state electronic structure is known with precision, its superconductivity remains

unexplained. There is evidence that its order parameter is chiral, but reconciling this with recent observations of the spin part of the pairing requires an order parameter that is either fine-tuned or implies a new form of pairing. Therefore, a definitive resolution of whether or not the superconductivity of $\mathbf{Sr_2RuO_4}$ is chiral is important for the study of superconductivity. Here, we report measurement of zero-field muon spin relaxation, a probe sensitive to weak magnetism, on samples under uniaxial stresses. We observe a stress-induced splitting between the onset temperatures of superconductivity and time reversal symmetry breaking - consistent with qualitative expectations for a chiral order parameter - and argue that this observation cannot be explained by conventional magnetism. In addition, we report the appearance of bulk magnetic order under higher uniaxial stress, above the critical pressure at which a Lifshitz transition occurs in $\mathbf{Sr_2RuO_4}$.

For most of its history, the superconductivity of Sr_2RuO_4 [1] has been understood in terms of an odd-parity, two-component order parameter with equal spin pairing in the RuO_2 planes: $p_x \pm ip_y$ [2, 3, 4, 5]. This order parameter is chiral: the Cooper pairs have angular momentum $l = \pm 1$. Evidence for chirality comes from ZF-μSR data [6], observation of a nonzero Kerr rotation below T_c [7], and signs in junction experiments of domains in the superconducting state [8, 9], while evidence for equal spin pairing came from the absence of a change in Knight shift below the critical temperature T_c in nuclear magnetic resonance (NMR) [10] and polarised-neutron scattering [11] measurements. The Knight shift is related to the spin susceptibility, and in conventional, opposite-spin-pairing superconductors it is suppressed below T_c. However, in new measurements it has been found that the Knight shift is in fact suppressed below T_c [12, 13, 14] by a magnitude that is unlikely to be reconcilable with equal spin pairing. This revision has called into question a number of other results on Sr_2RuO_4. It raises a particular challenge for experiments that indicate chirality, because opposite-spin pairing implies an even-parity momentum-space gap structure, and if the order parameter is constrained to be even-parity, chiral, and comprised of components that are degenerate on the tetragonal lattice of Sr_2RuO_4, the only possibility is $d_{xz} \pm id_{yz}$ order. Under conventional understanding this is a highly unlikely order parameter because it contains a horizontal line node at $k_z = 0$, and therefore implies pairing that is dominated by interlayer coupling. That would be a surprise because the interlayer coupling in Sr_2RuO_4 is weak: the ratio of inter- to intra-layer resistivity is of the order of 1000 [2]. Therefore, the question of whether or not the superconductivity of Sr_2RuO_4 is chiral has become highly important, because a confirmation may compel consideration of new forms of pairing.

At present, the evidence on chirality, and on time reversal symmetry breaking (TRSB) superconductivity more generally, is mixed. Scanning tunnelling microscopy data suggest a $d_{x^2-y^2}$ gap [15]. In scanning SQUID microscopy measurements magnetic fields on the scale indicated by ZF-μSR data have not been found [16]. A recent junction experiment finds time-reversal invariant superconductivity [17]. Furthermore, under in-plane uniaxial stress the tetragonal lattice symmetry of Sr_2RuO_4 is lifted, and consequently the degeneracy of the two components of $d_{xz} \pm id_{yz}$ or $p_x \pm ip_y$ order is expected to be lifted, yielding a split transition [18]; a schematic phase diagram is shown in Fig. 1(a). Evidence for this splitting has been resolved neither in heat capacity measurements under uniaxial stress [19], nor in the stress dependence of T_c [20, 21].

There is, however, no widely-accepted alternative hypothesis explaining the experiments that do indicate chirality. If the heat capacity anomaly associated with the second transition is small, its effects would be difficult to resolve in the uniaxial stress experiments that have been performed so far. Therefore, here we apply ZF-μSR, a non-thermodynamic probe specifically sensitive to time reversal symmetry breaking, to test for transition splitting under uniaxial stress. The signal that indicates TRSB superconductivity in unstressed Sr_2RuO_4 is an increase in the relaxation rate of implanted spin-polarised muons, an indicator of internal magnetic fields, below T_c. Although the reproducibility of this signal is well-established [6, 22, 23, 24], the difficulty in reconciling conflicting results in Sr_2RuO_4 has raised questions on whether it truly originates in TRSB superconductivity. One major goal of our experiment here is to rule out that it is an artefact of a conventional superconducting transition by some as-yet undetermined mechanism. We achieve this by showing that stress induces a clear splitting between T_c and T_{TRSB}, the onset temperature of enhanced muon spin relaxation. Furthermore, we show that stress exceeding 1 GPa induces magnetic order in Sr_2RuO_4, and that the signal in this state differs qualitatively from that below T_{TRSB} in unstressed Sr_2RuO_4, providing evidence that the enhanced muon spin relaxation at lower stresses is *not* a consequence of conventional magnetism. These results together provide strong support for a two-component superconducting order parameter that breaks time reversal symmetry in Sr_2RuO_4.

The essential experiment setup is shown schematically in Fig. 1(b). The sample is a plate thick enough to stop the muon beam, mounted in a holder that facilitates application of force. Concentric coils are mounted behind the sample, for in situ measurement of T_c through the Meissner effect. Hematite masks, whose internal magnetism rapidly depolarises muon spins that implant into them, screen portions of the holder that intrude into the beam. The muon spin is parallel to the beam direction, and to the c-axis of all the samples. A photograph of a sample holder is shown in Fig. ED1.

We first show results for unstressed Sr_2RuO_4. We compare ZF-μSR data, extended to temperatures well above T_c, with heat capacity data. Our results confirm previous observations [6, 22, 23, 24], and also show with high certainty that no spin relaxation enhancement is seen above T_c. Four samples, labelled A–D, were measured at zero stress. Samples A, C, and D have T_c = 1.38, 1.35, and 1.39 K respectively, close to the clean-sample limit of 1.50 K [25], while Sample B has T_c = 1.22 K.

In the μSR method, spin-polarised muons are implanted into the sample, where each muon spin then precesses in its local field. The measured quantity is the decay positron emission asymmetry $A(t)$, which is proportional to the muon spin polarisation at time t. $A(t)$ is conventionally obtained by direct comparison of the positron count rates in two detectors. Here, we instead analyse the count rates in each of the two detectors individually ("single histogram analysis"), an analysis method that reduces sensitivity to instrumentation drift. $A(t)$ for Sample B at two temperatures, one above and one well below T_c, are shown in Fig. 2. Slow muon spin relaxation is observed at the higher T, and faster relaxation at the lower T. External fields are compensated to better than 2 μT, so this change is not a consequence of the appearance of vortices. Muon spin relaxation is generally classified as exponential or gaussian, depending on whether relaxation is (exponential) or is not (gaussian) visible at short times; exponential relaxation corresponds to a broader internal field distribution [6]. In Sr_2RuO_4, the relaxation enhancement is exponential, meaning that $A(T < T_{\mathrm{TRSB}})/A(T > T_{\mathrm{TRSB}})$ decreases from short times and can be fitted well by an exponential form.

The muon spin relaxation rate λ at each temperature is obtained by fitting:

$$A_{\mathrm{fit}}(T,t) = A_{\mathrm{sam}} e^{-\lambda(T)t} + A_{\mathrm{bkg}}. \tag{1}$$

A_{bkg} is a background constant to account for muons that implant into background material such as cryostat walls, and A_{sam} is the sample signal strength. We make the simplifying assumption that A_{bkg} is t-independent— in other words, that the background muon spins do not relax. For all samples in this paper, A_{bkg} and A_{sam} are determined from separate transverse-field μSR measurements (see Fig. ED2), and therefore in the analysis of ZF data λ is the sole free fitting parameter. For all samples, $A_{\mathrm{bkg}} \ll A_{\mathrm{sam}}$. Results are shown in Fig. 2(b–d) for samples A-C and in Fig. 3(f) for sample D. In each sample, λ is seen to increase at low temperature. Phenomenological fits yield $T_{\mathrm{TRSB}} = 1.30 \pm 0.06$ K for Sample A, 1.3 ± 0.1 K for Sample B, 1.03 ± 0.08 K, for Sample C, and 1.37 ± 0.08 K for Sample D. (All error bars are one standard deviation.)

Although the fraction of background muons is small, we show in Fig. ED3 that different assumptions about the background relaxation rate strongly affect the absolute values of λ obtained in the single histogram analysis. As long as the background relaxation is T-independent, it is a uniform shift of $\lambda(T)$. In effect, when knowledge of the background is imperfect, the single histogram analysis improves sensitivity to small T-dependent changes in λ at the expense of greater uncertainty in absolute values, which therefore should not be compared across samples. We also show in Fig. ED3 a comparison of measurements of two similar samples, which shows that the background is, as hypothesised, T-independent, and in Fig. ED4 a control measurement in which the sample was covered with hematite, that confirms that the increase in λ below T_{TRSB} is a property of the Sr_2RuO_4.

Sample B has the same T_{TRSB} within error as samples A and D, in spite of its lower bulk T_c. However, susceptibility measurements reveal that T_c of Sample B is not homogeneous: the transition in susceptibility is broad and 0.25 K above the transition seen in heat capacity, likely due to internal strains that locally induce higher T_c [26, 27]. (These data, and further characterisation data for all samples, are shown in Fig. ED5.) T_{TRSB} of Sample C in contrast is distinctly below its T_c. Such splitting has not been reported before. It shows that there is a mechanism, not seen in most crystals, by which T_{TRSB} can be suppressed, but so far there is no evidence that T_{TRSB} can exceed T_c. We discuss this point in greater detail later.

Three samples (D–F) were measured under uniaxial stress. The unixial stress dependence of T_c of Sr_2RuO_4 is dominated by a stress-induced Fermi surface topological transition (a Lifshitz transition), that occurs at a stress σ applied along an Ru-O-Ru bond direction of -0.70 GPa [28, 29]. (Negative values of stress denote compression.) T_c peaks sharply at this stress, at a value of 3.5 K, while the upper critical field is enhanced by a factor of twenty [27].

Results for σ up to -0.86 GPa are shown in Fig. 3. Sample D was also measured at -0.28 and -0.43 GPa. A_{sam} and A_{bkg} were determined independently at each stress. In panels (a–c) it is seen that the relaxation enhancement remains exponential at each stress, and in panels (f–h), that T_{TRSB} remains low in spite of the stress-induced increase in T_c. Because the data here do not extend to very low temperatures (due to the poor thermal conductance of the pressure apparatus), a linear form is fitted to $\lambda(T)$ to extract T_{TRSB}:

$$\lambda = \begin{cases} \lambda_0 + b \times (T_{\mathrm{TRSB}} - T), & T < T_{\mathrm{TRSB}} \\ \lambda_0, & T > T_{\mathrm{TRSB}} \end{cases} \tag{2}$$

The slope b is a common fitting parameter among all three stresses, while T_{TRSB} and λ_0 are obtained independently at each stress. This fit gives $T_{\mathrm{TRSB}} = 1.37 \pm 0.08$ K at 0 GPa, 1.18 ± 0.06 K at -0.28 GPa, and 1.23 ± 0.08 K at -0.43 GPa. In other words, T_{TRSB} appears to be initially suppressed. The probability that T_{TRSB} is lower at -0.28 than at 0 GPa is 98%.

Sample E was measured at -0.70 GPa, right at the peak in T_{c}. Adopting the same phenomenological fit as applied to Sample D with the same slope b, T_{TRSB} of Sample E at -0.70 GPa is found to be 1.24 ± 0.16 K. Samples E and F were both cut from Sample C, which had $T_{\mathrm{TRSB}}(\sigma = 0) = 1.03 \pm 0.08$ K, so this is a potential enhancement from the unstressed T_{TRSB}, but with low statistical confidence. T_{TRSB} of Sample F at $\sigma = -0.79$ GPa, slightly beyond the peak in T_{c}, is 0.82 ± 0.08 K. A single data point from Sample F at a yet higher stress, -0.86 GPa, indicates that the time-reversal symmetry breaking is still present.

Sample F was compressed yet further, to $\sigma = -1.05$ GPa. $A(t)$ at various temperatures is shown in Fig. 4(a). The oscillations are an unmistakable indication of magnetic order. To analyse the oscillation data, we fit the following form to $A(t)$:

$$A(t) = \alpha\, j_0(2\pi\gamma_\mu B_{\max} t) e^{-\lambda_{\mathrm{T}} t} + (1 - \alpha)\, e^{-\lambda_{\mathrm{L}} t}. \tag{3}$$

Here, j_0 is a zeroth-order Bessel function, which is the Fourier transform of the Overhauser field distribution, $p(B) \propto (B_{\max}^2 - B^2)^{-1/2}$, expected for an incommensurate spin density wave. A damped cosine form, expected for commensurate magnetic order or ferromagnetism, does not fit well (see Fig. ED6). B_{max} is the magnetic hyperfine field at the peaks of the SDW, and γ_μ the muon gyromagnetic ratio. α is the oscillating signal fraction due to muons experiencing magnetic hyperfine fields transverse to the initial muon spin polarization. Since the magnetic order can also generate longitudinal field components at individual muon sites, which do not cause muon spin precession, α is a lower bound on the magnetic volume fraction. λ_{T} and λ_{L} describe an additional static line broadening and a slow dynamical spin relaxation, respectively. The results of the fits are shown in Fig. 4. α saturates at 60 %, and $B_{\mathrm{max}}(T \to 0)$ is 5.5 ± 0.1 mT. Fitting $B_{\mathrm{max}}(T)$ gives a Néel temperature T_N of 6.86 K. As further evidence that the magnetic order is a spin density wave, no anomaly that would indicate ferromagnetism was detected in the susceptibility data at $T \sim 7$ K.

λ_T and λ_L strongly increase below 2 K. The effect can be seen directly in Fig. 4(a): more oscillations are resolvable at 2.19 than at 0.44 K. Susceptibility data [Fig. 4(d)] show that the sample is superconducting with the main part of the transition at $T_{\mathrm{c}} \sim 1$ K, which shows that this change may be a consequence of the coexistence of superconductivity and magnetism. (The superconducting transition becomes broad at high stresses; we attribute this to stress inhomogeneity and a steep dependence of T_{c} on stress.)

To estimate the ordered moment, we compare with the static magnetic order induced in unstressed Sr_2RuO_4 by Ti substition. The electronic structure of Sr_2RuO_4 introduces susceptibilities at multiple wavevectors [30, 31], and so the stress-induced order may have a substantially different wavevector than the substitution-induced order, however it provides a first point of comparison. The $T \to 0$ ordered moment of $Sr_2Ru_{0.91}Ti_{0.09}O_4$ is 0.3 μ_B/Ru [32, 33], and in ZF-μSR data the first minimum in $A(t)$ occurs at 0.2 μs [34]. The first minimum in $A(t)$

for the stress-induced order occurs at 1 μs, suggesting an ordered moment of the order of 0.06 μ_B/Ru.

Functional renormalization group calculations have predicted stress-induced magnetic order in stoichiometric Sr_2RuO_4, but onsetting before the Fermi surface transition at -0.70 GPa is reached [35]. The observed onset of magnetic order is clearly beyond the Lifshitz transition: the -0.86 GPa data point of Sample F falls between the peak in T_c and appearance of magnetic order. Our data are summarized by the phase diagram in Fig. 5.

We now discuss the stress-induced splitting between T_c and T_{TRSB} for $|\sigma| < 1.0$ GPa. The systematic splitting proves decisively that the enhanced muon spin relaxation is not an artefact of the superconducting transition alone, for example through interaction of magnetic defects or magnetic interactions with conventional superconductivity. As described above, we have performed control measurements that rule out that T_{TRSB} is an artefact of the apparatus or background. At first glance, the weak variation of T_{TRSB} up to $\sigma = -1.0$ GPa, and the observation of magnetic order beyond 1.0 GPa, suggest a possibility that the enhanced muon spin relaxation is a consequence of a magnetic transition, rather than a property of the superconductivity. We argue that this is very unlikely. The small size of the signal rules out that it is a bulk magnetic transition, for the ordered moment would be only of the order of 0.002 μ_B/Ru, an extremely weak magnetism very seldom observed in real materials. Although such a delicate magnetic order is in principle possible, it would not then be expected to have such a weak response to strain-tuning. The 0.10 μ_B/Ru magnetic order of the related compound $Sr_3Ru_2O_7$ is extraordinarily sensitive to uniaxial stress, responding strongly to stresses of order 0.1 GPa [36]. A more reasonable hypothesis is therefore that a precursor of the bulk order at $\sigma \leq -1.0$ GPa condenses around certain defect sites. In this case, however, these islands of magnetic order would grow and become more numerous as the bulk transition is approached, yet the magnitude of the muon spin relaxation enhancement does not increase as σ approaches -1.0 GPa, and T_{TRSB} does not grow towards 7 K.

A known mechanism that can give weak exponential muon spin relaxation is fluctuations of weak ferromagnetism, as seen in $YbNi_4P_2$ [37] and CeFePO [38]. However in these cases the fluctuations, and corresponding muon spin relaxation rate λ, decay gradually over an order-of-magnitude increase in temperature. The rounding of the transitions in $\lambda(T)$ seen in Fig. 2 is at most a few times 0.1 K, which could be explained by sample inhomogeneity. Furthermore, the possibility that the internal fields are fluctuating was tested with longitudinal field measurements in Ref. [6], which concluded that they are static. Spin glasses can also give exponential muon relaxation, but even dilute spin glasses give much stronger relaxation than that observed here [39]. Further possible magnetic mechanisms are discussed in Supplementary Information; we find none consistent with observations.

A potential non-magnetic mechanism that could give enhanced muon spin relaxation is a structural transition in which the muon stopping site is altered, altering the muon - nuclear dipole interaction. However, structural transitions at such low temperature are rare, and furthermore we show, in Fig. ED7, results of a muon Knight shift measurement at 8 T on unstressed Sr_2RuO_4. No change in the Knight shift or line width that could indicate a structural transition is observed below 4 K.

The absence of a plausible magnetic mechanism to explain the observed signal leads to the conclusion that enhanced muon spin relaxation most likely marks a transition of the superconducting state. Splitting between T_{c} and T_{TRSB} has been observed previously in a few materials, but not with the clarity attained here. In UPt_3, a splitting of approximately 0.05 K was observed [40], although enhanced muon spin relaxation was not seen at all in a later report [41]. In both $Ba_{1-x}K_xFe_2As_2$ and $Pr_{1-x}La_xPt_4Ge_{12}$ there is a potential splitting of a few kelvin [42, 43, 44], but resolution in both cases is limited by the transition widths and small scale of the increase in λ. The case of UPt_3 is particularly informative, as Kerr rotation, superconducting junction, and small-angle neutron scattering measurements [45, 46, 47] show that at low temperature its superconductivity is chiral, providing further evidence that time reversal symmetry-breaking superconductivity causes enhanced muon spin relaxation.

We now discuss the possibility of chiral, $d_{xz} \pm id_{yz}$ order. Recent ultrasound measurements give evidence for two-component superconductivity [48, 49], and although there are strong thermodynamic constraints on this order parameter, we now argue that there are plausible mechanisms to reconcile it with experimental data. The primary constraint is the absence of a resolvable second transition in heat capacity data on uniaxially stressed Sr_2RuO_4 [19]: experiments constrain any heat capacity jump at T_{TRSB} to be less than 5% as large as that at T_{c}. The physical meaning is that d_{xz} or d_{yz} order would be nearly degenerate with $d_{xz} \pm id_{yz}$, due to competition between the two components. In a Ginzburg-Landau model of a two-component order parameter, the ratio of the slopes $|dT_{\mathrm{TRSB}}/d\sigma|$ and $|dT_{\mathrm{c}}/d\sigma|$ is inverse to the ratio of heat capacity jumps at T_{TRSB} and T_{c} (see Supplemental Information), so this observation constrains $|dT_{\mathrm{TRSB}}/d\sigma|$ to be at least 20 times larger than $|dT_{\mathrm{c}}/d\sigma|$ in the limit $\sigma \to 0$, which is in apparent contradiction to the observation that T_{TRSB} is suppressed weakly, if at all, while T_{c} is strongly enhanced under uniaxial stress.

However, it is possible that the range of validity of the $\sigma \to 0$ limit is small. At small $|\sigma|$, a suppression of T_{TRSB} is probably observed, while at large $|\sigma|$ the dependence of T_c on σ is clearly non-linear, indicating that the small-σ limit no longer applies. Furthermore, if the chirality of the superconductivity of Sr_2RuO_4 is as thermodynamically fragile a phenomenon as data indicate then the effect of disorder must also be considered. It is known that the superconductivity of Sr_2RuO_4 is among the most disorder-sensitive [25], and disorder and fluctuations are predicted to round off the cusps predicted in the mean-field phase diagram [50, 51], potentially obscuring the intrinsic small-σ behavior.

Disorder could potentially explain the the observation that $T_{\mathrm{TRSB}} < T_c$ in some unstressed samples of Sr_2RuO_4. All samples grow along an in-plane direction, so extended defects such as dislocations and Ru inclusions could have a preferred orientation. Oriented defects could be more effective in suppressed T_{TRSB} than lattice strain because they introduce large-angle scattering, whereas strain does not. Therefore an observation of splitting in some unstressed samples does not rule out chiral order. A recent proposal of inter-orbital pairing provides a possible mechanism to obtain a $d_{xz} \pm id_{yz}$ order parameter. Inter-orbital pairing becomes a realistic possibility when spin-orbit and Hund's rule couplings are non-negligible in comparison with the Fermi energy; how strong they must be is a subject of debate [52, 53, 54]. As yet, there are no widely-accepted examples of this type of superconductivity. However, in Sr_2RuO_4 it allows the possibility that $d_{xz} \pm id_{yz}$ symmetry is encoded in local orbital degrees of freedom rather than the k dependence of the gap, such that interlayer pairing is no longer required.

Other recently-discussed even-parity order parameters that break time-reversal symmetry include $d \pm is$ [55] and $d \pm ig$ [56]. These order parameters require tuning to obtain $T_{\mathrm{TRSB}} \approx T_c$, but it is argued in Refs. [55] and [56] that such tuning is realistic. Stress is generically expected to affect the two components of either order parameter differently, so if they are tuned to $T_{\mathrm{TRSB}} \approx T_c$ at $\sigma = 0$, splitting is expected when $\sigma \neq 0$ [56, 57]. Furthermore, because the proposed degeneracy with these two order parameters is tuned rather than symmetry-protected, there are no thermodynamic constraints on the relative stress dependencies of T_{TRSB} and T_{c}.

Methods

Samples and sample holder for uniaxial stress. Single crystals of Sr_2RuO_4 were grown by a floating zone method [58]. Data from six samples, labelled A–F, are reported; Samples E and F were cut from Sample C after measurement of Sample C. Sample A grew along approximately a $\langle 110 \rangle$ lattice direction, and the rest of the samples along a $\langle 100 \rangle$ direction; it was necessary to select samples that grew approximately along a $\langle 100 \rangle$ direction in order to obtain samples of sufficient length along this direction for mounting in the uniaxial stress apparatus. With the exception of Sample C, all samples studied here were either cleaved or ground into plates, exposing the interior of the as-grown rod to the muon beam.

Samples were mounted into holders as shown in Figs. 1 and ED1 using Stycast 2850 epoxy. The epoxy layers were generally 50–100 μm thick. The beam is approximately 1 cm in diameter, and for a decent count rate the sample area facing the beam should be at least 10 mm^2; we had 15 mm^2 for Samples E and F, and 26 mm^2 for Sample D. For Samples E and F, three additional steps were taken to improve the chances of reaching high stresses without fracturing the sample. (1) They were cut at a 10° angle with respect to the ab plane, so that shear stresses in the sample do not align with cleave planes. (2) 10 μm-thick titanium foils were affixed to their surfaces with Stycast 1266. (3) The slots in the holder were chamfered, as shown in Fig. 1(b), to smooth the interface between the free and clamped portions of the sample.

Photographs of the sample holder are shown in Fig. ED1. The holders slot into a piezoelectric-driven device that we term the generator, that generates forces of up to 1000 N; it is described in detail in Ref. [59]. Each holder incorporates a sensor of the force applied to the sample, based on strain gauges (Tokyo Sokki CFLA-3-350-11), and the cell incorporates a mechanical mechanism allowing the sensor reading at the zero-force point, $\sigma = 0$, to be determined in situ. As mentioned above, the holders also incorporate susceptibility coils, that are sized to measure most of the exposed portion of the sample, for measurement of T_c. The applied field from the coils was of the order of 10 μT. Measured values of T_c were used to calibrate the force sensors, following the stress dependence reported in Ref. [28]. In addition, the generator incorporates a displacement sensor, and the force-displacement relationship of the sample can be monitored to check for mechanical damage to the sample, or epoxy that holds the sample, as stress is applied.

Transverse-field data, for background determination. Before each set of zero-field measurement the ratio $A_{\mathrm{bkg}}/A_{\mathrm{sam}}$ (See Eq. 1) was determined using transverse-field μSR. Here, we show some of this data. In Fig. ED2 transverse-field data from Sample D at 0 and -0.43 GPa are shown. The applied field was 14.5 mT, and above T_c the muons precess without strong relaxation in this field. This field was applied along the c axis, where $H_{c2}(T \to 0) \approx 70$ mT, and below T_c the field within the sample becomes highly inhomogeneous due to the vortex lattice. Correspondingly, well below T_c the polarization of muon spins implanted in the sample relaxes rapidly. At -0.43 GPa, it can be seen however that there is residual oscillation that appears not to relax. This is due to the background muons, that implant into material other than the sample and so see a uniform field. To fit $A(t)$, we assume a field distribution that is a sum of a few Gaussians, with one describing the background and the rest the vortex lattice [60]. $A(t)$ is fitted in the time domain to a Fourier transform of this assumed field distribution. Results are shown in panels (c) and (d). By comparing the fitted amplitudes of the background and vortex contributions, we obtain $A_{\text{bkg}}/A_{\text{sam}} \approx 0.12$ for Sample D at -0.43 GPa.

For Sample D at 0 and -0.28 GPa, $A_{\text{bkg}}/A_{\text{sam}}$ was 0.05. The increase between -0.28 and -0.43 GPa is due to a chip that broke from the sample as the applied stress was increased, which exposed a portion of the susceptibility coils to the muon beam. For the remaining samples, $A_{\text{bkg}}/A_{\text{sam}}$ came to approximately 0 for Samples A, B, and F; 0.12 for Sample C; and 0.15 for Sample E.

Analysis of μSR data. We now provide more information on the μSR technique, and in particular the single histogram analysis method that was employed here. We first explain the analysis, and then illustrate its sensitivity to assumptions about the background. We show that as long as the background relaxation is T-independent, T-dependent changes in λ from the sample are obtained accurately, and then show an experimental demonstration that a T-independent background is a valid assumption.

Measurements were performed with 4.2 MeV muons, which penetrate to a depth of $\sim$0.1 mm, using the Dolly instrument on the πE1 beamline at the Paul Scherrer Institute. The spin polarisation of the muons was parallel to the beam. Conventionally, the count rates of decay positrons in two detectors (here, one forward and the other backward along the muon beam) are compared directly to obtain $A(t)$:

$$A(t) = \frac{(N_1(t) - N_{\text{dark},1}) - (N_2(t) - N_{\text{dark},2})}{(N_1(t) - N_{\text{dark},1}) + (N_2(t) - N_{\text{dark},2})}$$

where $N_i(t)$ is the number of counts in detector i at time t. At the Paul Scherrer Institute, the rate at which muons enter the system is typically adjusted so that there is seldom more than one muon in the sample at a time. As the muon enters the sample area, it is detected by an upstream detector that triggers the timer that records the time t. $N_{\text{dark},i}$ is the "dark" count rate of each detector, due to uncorrelated events in the upstream trigger muon detector and the positron detector.

We obtained $A(t)$ in this conventional way for the transverse-field data, where A varies rapidly with time. However, when relaxation is slow, as it is for Sr_2RuO_4, the fitted relaxation rates λ become sensitive to errors in the dark rates, and so for the ZF data rather than comparing count rates in the two detectors the counts in each detector was analysed individually, with $N_{\text{dark},i}$ as a fitting parameter [43]. Each count rate $N_i(t)$ is fitted by

$$N_i(t) = N_{0,i}[1 + A_{\text{fit},i}(t)]e^{-t/\tau_\mu} + N_{\text{dark},i},$$

where τ_μ is the muon lifetime, $N_{0,i}$ is a fitting parameter setting the overall number of counts, and $A_{\text{fit},i}(t)$ is the hypothesised functional form of the muon spin relaxation. We take $A_{\text{fit},i}(t) = A_{\text{sam},i}e^{-\lambda t} + A_{\text{bkg},i}$. $A_{\text{sam},i}$ and $A_{\text{bkg},i}$ are obtained from separate transverse-field measurements. $A_{\text{sam},1}$ and $A_{\text{sam},2}$ have opposite sign, due to the initial muon polarisation. The relaxation rate λ is determined from fits to both detector signals simultaneously, using the MUSRFIT program [61].

We plot in Figs. 2–4 the experimental asymmetry data points as $A(t) \equiv \frac{1}{2}[A_1(t) - A_2(t)]$, where

$$A_i(t) = \frac{N_i(t) - N_{\mathrm{dark},i}}{N_{0,i} \exp(-t/\tau_\mu)} - 1.$$

These are compared with the model asymmetry function $A_{\mathrm{fit}}(t) \equiv \frac{1}{2}[A_{\mathrm{fit},1}(t) - A_{\mathrm{fit},2}(t)]$. In the single histogram analysis it is unavoidable that the experimental $A(t)$ depends on the model $A_{\mathrm{fit}}(t)$, because a model is required to obtain $N_{\mathrm{dark},i}$. We emphasise however that the procedure is not "self-adjusting:" agreement between $A(t)$ and $A_{\mathrm{fit}}(t)$ is not obtained if an inappropriate $A_{\mathrm{fit}}(t)$ is selected; see Fig. ED6, an analysis of the magnetic order, for an example.

For simplicity, a non-relaxing (that is, time-independent) background A_{bkg} was assumed for all samples. We now show that assuming a different form of background strongly changes the absolute values of λ obtained from the single-histogram analysis, but negligibly affects relative values. For Sample D, as stress was increased from -0.28 to -0.43 GPa a chip broke from the sample, exposing some brass material behind the sample to the beam, which, due to the nuclear magnetic moments of Cu, is strongly relaxing. The relaxation from copper can be accurately fit by the Gauss-Kubo-Toyabe form with $\sigma = 0.39$ $\mu\mathrm{s}^{-1}$ [62]. In Fig. ED3(a) we show two sets of results for $A(t)$ of Sample D at -0.43 GPa, taking for one a non-relaxing background, and for the other a background in which 55% of the background muon spins relax following the expected muon spin relaxation function of copper while the remaining 45% do not relax. Panel (b) shows the resulting relaxation rates λ, which are seen to be considerably lower when a relaxing background is assumed. However, when temperature-independent constants are subtracted in panel (c), the effect of assuming a different background on relative values of λ is seen to be negligible. We analyse data assuming non-relaxing backgrounds because it is not realistic to accurately determine the true background relaxation rate for each sample.

For a direct experimental verification that the background does not affect the observed T_{TRSB} or the magnitude of the change in λ below T_{TRSB}, we perform measurements of an additional sample, Sample A2. Samples A and A2 were about 1.5 cm apart in the same original rod of Sr_2RuO_4, and have nearly identical T_{c}. Sample A2 was mounted into the uniaxial stress apparatus, but force was not applied. Transverse-field data, shown in Fig. ED3(d), show that about 13% of the muons implant into background material. In panel (e), it is shown that Samples A and A2 have nearly identical heat capacities and critical temperatures. The absolute value of muon spin relaxation rate λ obtained from the single histogram analysis differs strongly between the two samples, which as described above is almost certainly an artefact of the fact that Sample A2 was mounted in the stress apparatus while Sample A was not, rather than an actual difference in the samples. Crucially, very similar values for T_{TRSB} and the change in λ below T_{TRSB} are obtained from both samples.

Control measurement. As noted in the main text, hematite plates are used to mask sections of the holder in the beam: the strong antiferromagnetism of hematite relaxes the polarization of muon spins that implant into these masks within 50 ns, allowing these muons to be excluded from analysis. Being antiferromagnetic, the masks do not generate long-range stray fields.

To verify that the enhanced muon spin relaxation below T_{TRSB} is not an artefact of background material or the hematite masks, we performed the experiments with the sample covered with hematite as shown in Fig. ED4(a). In Fig. ED4(b) one can see $A(t)$ from the first 50 ns. This fastly oscillating signal is due to muons that implant into the hematite. The asymmetry can be fitted by a damped cosine. It decays very rapidly, and the remaining asymmetry is due to muons that implanted into material other than the hematite, or into paramagnetic portions of the hematite masks. In panel (c), measurements under a weak transverse field are shown. The initial asymmetry is approximately 0.027, whereas it is approximately 0.27 when all the muons implant into a non-magnetic, non-relaxing material, which shows that about 10% of the muons implant into background material. In panel (d), we show asymmetry time spectra from zero-field measurements for a longer time interval. The polarisation of these background muon spins relaxes on a time scale of several μs. The temperature dependence of this relaxation rate is shown in panel (e): no significant change is resolved, which shows that in the measurements on Sr_2RuO_4 the observed relaxation rate enhancement is due to the Sr_2RuO_4, and not an artifact of the background material or the hematite mask.

Additional sample characterization data. Additional characterization data of the samples are shown in Fig. ED5. Heat capacity data are shown for all samples except Sample F; Samples E and F were both drawn from Sample C, and so are expected to have very similar properties. The samples have sharp transitions with T_c near the clean-sample limit of 1.50 K in all samples except Sample B. For Samples D and E, T_c and the transition widths obtained from heat capacity and susceptibility data match closely, indicating high sample homogeneity, while for Sample B the transition in susceptibility is broad and at a higher temperature than the heat capacity transition, most likely due to internal defects such as Ru inclusions, which locally increase T_c through strain effects.

To obtain a superconducting penetration depth we performed transverse field measurements at various temperatures across T_c. In the superconducting state the data were analyzed by a multi-Gaussian fit to obtain the second moment of the internal field distribution in the vortex state, as described in Ref. [60]. The penetration depth λ was calculated using the Brandt relation between the magnetic penetration depth and the second moment $\langle \Delta B^2 \rangle = 0.00371\, \Phi_0^2/\lambda^4$, valid for the case when the applied field $B << B_{\mathrm{c2}}$ [63], where Φ_0 in the magnetic flux quantum. The latter holds for the data presented in Fig. ED5, where the inverse squared penetration depth λ^{-2} is plotted. The measurements shown in panel (a), (f), and (g) were performed with B$\|$ $c = 2$ mT, yielding the in-plane superfluid density λ_{ab}^{-2}, and in panel (c) with B$\|$ $ab = 14.5$ mT, yielding $(\lambda_{ab}\lambda_c)^{-1}$. Like the heat capacity data of Ref. [19], these measurements show definitively that the strain-induced increase in T_{c} is a bulk effect.

Additional analysis of the magnetic phase. As described in the main text, the internal field distribution in the magnetic state is well-described by a Bessel function, which is the field distribution expected for an incommensurate spin density wave. We show here that ferromagnetism does not give as good a match; we analyse this alternative possibility because ferromagnetism is a generally likely consequence of tuning materials to peaks in the density of states. The expected functional form for $A(t)$ for ferromagnetism is a cosine:

$$A(t) = \alpha\, \cos(2\pi\gamma_\mu Bt)e^{-\lambda_{\mathrm{T}}t} + (1-\alpha)\, e^{-\lambda_{\mathrm{L}}t},$$

where B is now the average local magnetic field at the muon site induced by the magnetism, and other quantities are as in the main text. For uniform ferromagnetism, non-relaxing precession is expected, and the damping parameters λ_{T} and λ_{L} describe the width of the field distribution. This form also applies to commensurate magnetic order: reversing the field direction on every other site would not alter $A(t)$. Results are shown in Fig. ED6. The cosine fit does not reproduce the data at early time ($t \lesssim 0.1\mu$s) or at $t > 2\mu$s. In particular, it does not capture the third peak in $A(t)$, at $t \approx 3.2$ μs, which is clearly present not only here (at $T = 2.9$ K), but also in the 2.19 and 4.4 K data in Fig. 4(a).

Alternative forms for $A(t)$. The exponential form to which we fit $A(t)$ is taken as a phenomenological form that accurately captures our data. For static, randomly distributed dilute field sources, the Lorentzian Kubo-Toyabe function, $f_{\mathrm{LKT}} = \frac{1}{3} + \frac{2}{3}(1-\lambda t)e^{-\lambda t}$, is generally a more accurate description, however we found no improvement in our fits and, in the absence of a widely-accepted microscopic model for the internal fields, use the simpler fitting instead. The field from nuclear dipoles, which is a dense field source, is generally described by the Gaussian-Kubo-Toyabe function, $f_{\mathrm{GKT}} = \frac{1}{3} + \frac{2}{3}(1-\sigma^2 t^2)\exp(-\frac{1}{2}\sigma^2 t^2)$. Therefore another form that may be employed for fitting is $A(t) = f_{\mathrm{GKT}}(t) \times e^{-\lambda t}$, where the added exponential describes the additional relaxation below T_{TRSB}. We tested a simpler phenomenological form on Sample D, $A(t) = A_{\mathrm{bkg}} + A_{\mathrm{sam}}\exp(-\lambda t)\exp(-\frac{1}{2}\sigma^2 t^2)$, but found that the fit quality was not improved by adding the extra fitting parameter.

High-resolution Knight shift measurements. To investigate whether the anomaly at $T \sim 1.5$ K is observed in the normal state, we performed high-resolution Knight shift measurements as proposed in Ref. [64]. The field was applied in the ab-plane, and as in our zero-field measurements the muon spin was parallel to the c-axis. The sample was cut from the sample A2 and had a cylindrical shape with a diameter of 3 mm and height of 2 mm. The Knight shift is defined relative to an Ag reference, and correction for diamagnetic effects was not performed. The data were fitted in the time domain using two cosine components with exponential damping. The result is summarized in Fig. ED7: no change in Knight shift or relaxation rate is resolved below 4 K.

Data Availability Statement

The data are represented in Figs. 2-5 are available as Source Data. All other data that support the plots within this paper and other findings of this study are available from the corresponding authors upon reasonable request.

Acknowledgment

This work has been supported financially by the Deutsche Forschungsgemeinschaft (GR 4667/1, GRK 1621, and SFB 1143 projects C02 and C09) and the Max Planck Society. YM, TM, and JB acknowledge the financial support of JSPS Kakenhi (JP15H5852, JP15K21717, and JP17H06136) and the JSPS Core-to-Core Program. NK acknowledges the financial support from JSPS Kakenhi (No. JP18K04715) and JST-Mirai Program (No. JPMJMI18A3). AN acknowledges funding from the European Union's Horizon 2020 research and innovation program under the Marie Sklodowska-Curie grant agreement No 701647. This work was performed partially at the Swiss Muon Source (SμS), PSI, Villigen. We acknowledge fruitful discussions with A. Amato, B. Andersen, E. Babaev, S. Blundell, A. Charnukha, D. Efremov, I. Eremin, C. Kallin, A. Ramires, B. Ramshaw, A. Rømer, T. Scaffidi, M. Sigrist, C. Timm and S. Yonezawa. We also acknowledge H.-S. Xu for his contribution in the crystal growth as well as T. Shiroka and C. Wang for technical support. We thank A. Gilman, P. P. Orth, and R. M. Fernandes for results from Landau theory of a two-component order parameter.

Authors contribution

V. G., S. G., R. S., J.-C. O., A. N., D. D., Z. G., H. L., and H.-H. K. performed the μSR measurements. V. G. performed the heat capacity measurements. V. G., S. G., H. L. analysed the raw μSR data. S. G., A. N., M. E., F. B., and C. W. H. built and characterised the stress apparatus. M. E. B. and J. P. characterised samples. N. K., D. A. S., J. S. B., and T. M. grew samples. V. G., Y. M., A. P. M., H. L., C. W. H. and H.-H. K. supervised the research. V. G., C. W. H., and H.-H. K. wrote the paper. C. W. H. designed the stress apparatus. H.-H. K. initiated this study. All authors discussed the results and implications, and commented on the manuscript.

Competing interests

The authors declare no competing financial interests.

Additional information

Supplementary information is available for this paper.

References

[1] Maeno, Y., Hashimoto, H., Yoshida, K., Nishizaki, S., Fujita, T., Bednorz, J., and Lichtenberg, F. Superconductivity in a layered perovskite without copper. *Nature* **372**, 532–534 (1994).

[2] Mackenzie, A. P. and Maeno, Y. The superconductivity of Sr_2RuO_4 and the physics of spin-triplet pairing. *Reviews of Modern Physics* **75**, 657–712 (2003).

[3] Mackenzie, A. P., Scaffidi, T., Hicks, C. W., and Maeno, Y. Even odder after twenty-three years: the superconducting order parameter puzzle of Sr_2RuO_4. *npj Quantum Materials* **2**, 40 (2017).

[4] Maeno, Y., Kittaka, S., Nomura, T., Yonezawa, S., and Ishida, K. Evaluation of Spin-Triplet Superconductivity in Sr_2RuO_4. *J. Phys. Soc. Jpn.* **81**, 011009 (2012).

[5] Kallin, C. Chiral p-wave order in Sr_2RuO_4. *Reports on Progress in Physics* **75**, 042501 (2012).

[6] Luke, G. M., Fudamoto, Y., Kojima, K. M., Larkin, M. I., Merrin, J., Nachumi, B., Uemura, Y. J., Maeno, Y., Mao, Z. Q., Mori, Y., Nakamura, H., and Sigrist, M. Time-reversal symmetry-breaking superconductivity in Sr_2RuO_4. *Nature* **394**, 558–561 (1998).

[7] Xia, J., Maeno, Y., Beyersdorf, P. T., Fejer, M. M., and Kapitulnik, A. High Resolution Polar Kerr Effect Measurements of Sr_2RuO_4: Evidence for Broken Time-Reversal Symmetry in the Superconducting State. *Phys. Rev. Lett.* **97**, 167002 (2006).

[8] Nakamura, T., Sumi, T., Yonezawa, S., Terashima, T., Sigrist, M., Kaneyasu, H., and Maeno, Y. Essential Configuration of Pb/Ru/Sr_2RuO_4 Junctions Exhibiting Anomalous Superconducting Interference. *J. Phys. Soc. Jpn.* **81**, 064708 (2012).

[9] Anwar, M. A., Nakamura, T., Yonezawa, S., Yakabe, M., Ishiguro, R., Takayanagi, H., and Maeno, Y. Anomalous switching in Nb/Ru/Sr_2RuO_4 topological junctions by chiral domain wall motion. *Scientific Reports* **3**, 2480 (2013).

[10] Ishida, K., Mukuda, H., Kitaoka, Y., Asayama, K., Mao, Z. Q., Mori, Y., and Maeno, Y. Spin-triplet superconductivity in Sr_2RuO_4 identified by ^{17}O Knight shift. *Nature* **396**, 658–660 (1998).

[11] Duffy, J. A., Hayden, S. M., Maeno, Y., Mao, Z., Kulda, J., and McIntyre, G. J. Polarized-Neutron Scattering Study of the Cooper-Pair Moment in Sr_2RuO_4. *Phys. Rev. Lett.* **85**, 5412 (2000).

[12] Pustogow, A., Luo, Y., Chronister, A., Y.-S., S., Sokolov, D. A., Jerzembeck, F., Mackenzie, A. P., Hicks, C. W., Kikugawa, N., Raghu, S., Bauer, E. D., and Brown, S. E. Constraints on the superconducting order parameter in Sr_2RuO_4 from oxygen-17 nuclear magnetic resonance. *Nature* **574**, 72–75 (2019).

[13] Ishida, K., Manago, M., and Maeno, Y. Reduction of the 17O Knight Shift in the Superconducting State and the Heat-up Effect by NMR Pulses on Sr_2RuO_4. *J. Phys. Soc. Jpn.* **89**, 034712 (2020).

[14] Petsch, A. N., Zhu, M., Enderle, M., Mao, Z. Q., Maeno, Y., and Hayden, S. M. Reduction of the spin susceptibility in the superconducting state of Sr_2RuO_4 observed by polarized neutron scattering. *Phys. Rev. Lett.* **125**, 217004 (2020).

[15] Sharma, R., Edkins, S. D., Z., W., Kostin, A., Saw, C., Maeno, Y., Mackenzie, A. P., Davis, J. C., and Madhavan, V. Momentum-resolved superconducting energy gaps of Sr_2RuO_4 from quasiparticle interference imaging. *PNAS* **117 (10)**, 5222-5227 (2020).

[16] Hicks, C. W., Kirtley, J. R., Lippman, T. M., Koshnick, N. C., Huber, M. E., Maeno, Y., Yuhasz, W. M., Maple, M. B., and Moler, K. A.Limits on superconductivity-related magnetization in Sr_2RuO_4 and $PrOs_4Sb_{12}$ from scanning SQUID microscopy. *Phys. Rev. B* **81**, 214501 (2010).

[17] Kashiwaya, S., Saitoh, K., Kashiwaya, H., Koyanagi, M., Sato, M., Yada, K., Tanaka, Y., and Maeno, Y. Time-reversal invariant superconductivity of Sr_2RuO_4 revealed by Josephson effects. *Phys. Rev. B* **100**, 094530 (2019).

[18] Sigrist, M. and Ueda, K. Phenomenological theory of unconventional superconductivity. *Rev. Mod. Phys.* **63**, 239–311 (1991).

[19] Li, Y.-S., Kikugawa, N., Sokolov, D. A., Jerzembeck, F., Gibbs, A. S., Maeno, Y., Hicks, C. W., Nicklas, M., and Mackenzie, A. P. High sensitivity heat capacity measurements on Sr_2RuO_4 under uniaxial pressure. *arXiv:1906.07597* (2019).

[20] Hicks, C. W., Brodsky, D. O., Yelland, E. A., Gibbs, A. S., Bruin, J. A. N., Barber, M. E., Edkins, S. D., Nishimura, K., Yonezawa, S., Maeno, Y., and Mackenzie, A. P. Strong Increase of T_c of Sr_2RuO_4 Under Both Tensile and Compressive Strain. *Science* **344**, 283-285 (2014).

[21] Watson, C. A., Gibbs, A. S., Mackenzie, A. P., Hicks, C. W., and Moler, K. A. Micron-scale measurements of low anisotropic strain response of local T_c in Sr_2RuO_4. *Phys. Rev. B* **98**, 094521 (2018).

[22] Shiroka, T., Fittipaldi, R., Cuocco, M., De Renzi, R., Maeno, Y., Lycett, R. J., Ramos, S., Forgan, E. M., Baines, C., Rost, A., Granata, V., and Vecchione, A. μSR studies of superconductivity in eutectically grown mixed ruthenates. *Phys. Rev. B* **85**, 134527 (2012).

[23] Luke, G. M., Fudamoto, Y., Kojima, K. M., Larkin, M. I., Nachumi, B., Uemura, Y. J., Sonier, J. E., Maeno, Y., Mao, Z. Q., Mori, Y., and Agterberg, D. F. Unconventional superconductivity in Sr_2RuO_4. *Physica B* **289-290**, 373-376 (2000).

[24] Higemoto, W., Koda, A., Kadono, R., Yoshida, Y., and Onuki, Y. Investigation of Spontaneous Magnetic Field in Spin-Triplet Superconductor Sr_2RuO_4. *JPS Conference Proceedings* **2**, 010202 (2014).

[25] Mackenzie, A. P., Haselwimmer, R. K. W., Tyler, A. W., Lonzarich, G. G., Mory, Y., Nishizaki, S., and Maeno, Y. Extremely Strong Dependence of Superconductivity on Disorder in Sr_2RuO_4. *Phys. Rev. Lett.* **80**, 161–164 (1998).

[26] Maeno, Y., Ando, T., Mori, Y., Ohmichi, E., Ikeda, S., Nishizaki, S., and Nakatsuji, S. Enhancement of Superconductivity of Sr_2RuO_4 to 3 K by Embedded Metallic Microdomains. *Phys. Rev. Lett.* **81**, 3765–3768 (1998).

[27] Steppke, A., Zhao, L., Barber, M. E., Scaffidi, T., Jerzembeck, F., Rosner, H., Gibbs, A. S., Maeno, Y., Simon, S. H., Mackenzie, A. P., and Hicks, C. W. Strong peak in Tc of Sr_2RuO_4 under uniaxial pressure. *Science* **355**, eaaf9398 (2017).

[28] Barber, M. E., Lechermann, F., Streltsov, S. V., Skornyakov, S. L., Ghosh, S., Ramshaw, B. J., Kikugawa, N., Sokolov, D. A., Mackenzie, A. P., Hicks, C. W., and Mazin, I. I. Role of correlations in determining the Van Hove strain in Sr_2RuO_4. *Phys. Rev. B* **100**, 245139 (2019).

[29] Sunko, V., Abarce Morales, E., Marković, I., Barber, M. E., Milosavljević, D., Mazzola, F., Sokolov, D. A., Kikugawa, N., Cacho, C., Dudin, P., Rosner, H., Hicks, C. W., King, P. D. C., and Mackenzie, A. P. Direct observation of a uniaxial stress-driven Lifshitz transition in Sr_2RuO_4. *npj Quantum Materials* **4**, 46 (2019).

[30] Steffens, P., Sidis, Y., Kulda, J., Mao, Z. Q., Maeno, Y., Mazin, I. I., and Braden, M. Spin Fluctuations in Sr_2RuO_4 from Polarized Neutron Scattering: Implications for Superconductivity. *Phys. Rev. Lett.* **122**, 047004 (2019).

[31] Cobo, S., Ahn, F., Eremin, I., and Akbari, A.Anisotropic spin fluctuations in Sr_2RuO_4: Role of spin-orbit coupling and induced strain. *Phys. Rev. B* **94**, 224507 (2016).

[32] Minakata, M. and Maeno, Y. Magnetic ordering in Sr_2RuO_4 induced by nonmagnetic impurities. *Phys. Rev. B* **63**, 180504 (2001).

[33] Braden, M., Friedt, O., Sidis, Y., Bourges, P., Minakata, M., and Maeno, Y. Incommensurate Magnetic Ordering in $Sr_2Ru_{1-x}Ti_xO_4$. *Phys. Rev. Lett.* **88**, 197002 (2002).

[34] Carlo, J. P., Goko, T., Gat-Malureanu, I. M., Russo, P. L., Savici, A. T., Aczel, A. A., MacDougall, G. J., Rodriguez, J. A., Williams, T. J., Luke, G. M., Wiebe, C. R., Yoshida, Y., Nakatsuji, S., Maeno, Y., Taniguchi, T., and Uemura, Y. J. New magnetic phase diagram of $(Sr,Ca)_2RuO_4$. *Nature Materials* **11**, 323–328 (2012).

[35] Liu, Y.-C., Zhang, F.-C., Rice, T. M., and Wang, Q.-H. Theory of the evolution of superconductivity in Sr_2RuO_4 under anisotropic strain. *npj Quantum Materials* **2**, 12 (2017).

[36] Brodsky, D. O., Barber, M. E., Bruin, J. A. N., Borzi, R. A., Grigera, S. A., Perry, R. S., Mackenzie, A. P., and Hicks, C. W. Strain and vector magnetic field tuning of the anomalous phase in $Sr_3Ru_2O_7$. *Science Advances* **3**, e1501804 (2017).

[37] Spehling, J., Günther, M., Krellner, C., Yèche, N., Luetkens, H., Baines, C., Geibel, C., and Klauss, H.-H. Magnetic order and spin dynamics in the proximity of a ferromagnetic quantum critical point: A μSR study of $YbNi_4P_2$. *Phys. Rev. B* **85**, 140406(R) (2012).

[38] Lausberg, S., Spehling, J., Steppke, A., Jesche, A., Luetkens, H., Amato, A., Baines, C., Krellner, C., Brando, M., Geibel, C., Klauss, H.-H., and Steglich, F. Avoided Ferromagnetic Quantum Critical Point: Unusual Short-Range Ordered State in CeFePO. *Phys. Rev. Lett.* **109**, 216402 (2012).

[39] Wu, W. D., Keren, A., Le, L. P., Luke, G. M., Sternlieb, B. J., Uemura, Y. J., Seaman, C. L., Dalichaouch, Y., and Maple, M. B. Muon spin relaxation studies of magnetic order in $Y_{1-x}U_xPd_3$ and UPd_4. *Phys. Rev. Lett.* **72**, 3722–3725 (1994).

[40] Luke, G. M., Keren, A., Le, L. P., Wu, W. D., Uemura, Y. J., Bonn, D. A., Taillefer, L., and Garrett, J. D. Muon spin relaxation in UPt_3. *Phys. Rev. Lett.* **71**, 1466–1469 (1993).

[41] Dalmas de Réotier, P., Huxley, A., Yaouanc, A., Flouquet, J., Bonville, P., Imbert, P., Pari, P., Gubbens, P. C. M., and Mulders, A. M. Absence of zero field muon spin relaxation induced by superconductivity in the B phase of UPt_3. *Physics Letters A* **205**, 239-243 (1995).

[42] Grinenko, V., Materne, P., Sarkar, R., Luetkens, H., Kihou, K., Lee, C. H., Akhmadaliev, S., Efremov, D. V., Drechsler, S.-L., and Klauss, H.-H. Superconductivity with broken time-reversal symmetry in ion-irradiated $Ba_{0.27}K_{0.73}Fe_2As_2$ single crystals. *Phys. Rev. B* **95**, 214511 (2017).

[43] Grinenko, V., Sarkar, R., Kihou, K., Lee, C. H., Morozov, I., Aswartham, S., Büchner, B., Chekhonin, P., Skrotzki, W., Nenkov, K., Hühne, R., Nielsch, K., Drechsler, S. L., Vadimov, V. L., Silaev, M. A., Volkov, P. A., Eremin, I., Luetkens, H., and Klauss, H.-H. Superconductivity with broken time-reversal symmetry inside a superconducting s-wave state. *Nat. Phys.* **16**, 789–794 (2020).

[44] Zhang, J., Ding, Z. F., Huang, K., Tan, C., Hillier, A. D., Biswas, P. K., MacLaughlin, D. E., and Shu, L. Broken time-reversal symmetry in superconducting $Pr_{1-x}La_xPt_4Ge_{12}$. *Phys. Rev. B* **100**, 024508 (2019).

[45] Schemm, E. R., Gannon, W. J., Wishne, C. M., Halperin, W. P., and Kapitulnik, A. Observation of broken time-reversal symmetry in the heavy-fermion superconductor UPt_3. *Science* **345**, 190-193 (2014).

[46] Strand, J. D., Bahr, D. J., Van Harlingen, D. J., Davis, J. P., Gannon, W. J., and Halperin, W. P. The Transition Between Real and Complex Superconducting Order Parameter Phases in UPt_3. *Science* **328**, 1368-1369 (2010).

[47] Avers, K. E., Gannon, W. J., Kuhn, S. J., Halperin, W. P., Sauls, J. A., DeBeer-Schmitt, L., Dewhurst, C. D., Gavilano, J., Nagy, G., Gasser, U., and Eskildsen, M. R. Broken time-reversal symmetry in the topological superconductor UPt_3. *Nat. Phys.* **16**, 531–535 (2020).

[48] Ghosh, S., Shekhter, A., Jerzembeck, F., Kikugawa, N., Sokolov, D. A., Mackenzie, A. P., Hicks, C. W., and Ramshaw, B. J. Thermodynamic evidence for a two-component superconducting order parameter in Sr_2RuO_4. *Nat. Phys.* (2020) https://doi.org/10.1038/s41567-020-1032-4.

[49] Benhabib, S., Lupien, C., Paul, I., Berges, L., Dion, M., Nardone, M., Zitouni, A., Mao, Z. Q., Maeno, Y., Georges, A., Taillefer, L., and Proust, C. Ultrasound evidence for a two-component superconducting order parameter in Sr_2RuO_4. *Nat. Phys.* (2020) https://doi.org/10.1038/s41567-020-1033-3.

[50] Fischer, M. H. and Berg, E.Fluctuation and strain effects in a chiral p-wave superconductor. *Phys. Rev. B* **93**, 054501 (2016).

[51] Yu, Y. and Raghu, S.Effect of strain inhomogeneity on a chiral p-wave superconductor. *Phys. Rev. B* **100**, 094517 (2019).

[52] Puetter, C. M. and Kee, H.-Y. Identifying spin-triplet pairing in spin-orbit coupled multi-band superconductors. *EPL* **98** 27010 (2012).

[53] Ramires, A. and Sigrist, M. Superconducting order parameter of Sr_2RuO_4: A microscopic perspective *Phys. Rev. B* **100**, 104501 (2019).

[54] Suh, H. G., Menke, H., Brydon, P. M. R., Timm, C., Ramires, A., and Agterberg, D. F. Stabilizing even-parity chiral superconductivity in Sr_2RuO_4. *Phys. Rev. Research* **2**, 032023(R) (2019).

[55] Rømer, A. T., Scherer, D. D., Eremin, I. M., Hirschfeld, P. J., and Andersen, B. M. Knight Shift and Leading Superconducting Instability from Spin Fluctuations in Sr_2RuO_4. *Phys. Rev. Lett.* **123**, 247001 (2019).

[56] Kivelson, S. A., C., Y. A., Ramshaw, B. J., and Thomale, R. A proposal for reconciling diverse experiments on the superconducting state in Sr_2RuO_4. *npj Quantum Mat.* **5**, 43 (2020).

[57] Rømer, A. T., A., K., Müller, M. A., Hirschfeld, P. J., Eremin, I. M., and Andersen, B. M. Theory of strain-induced magnetic order and splitting of T_c and T_TRSB in Sr_2RuO_4. *Phys. Rev. B* **102**, 054506 (2020).

[58] Bobowski, J. S., Kikugawa, N., Miyoshi, T., Suwa, H., Xu, H.-S., Yonezawa, S., Sokolov, D. A., Mackenzie, A. P., and Maeno, Y. Improved Single-Crystal Growth of Sr_2RuO_4. *Condensed Matter* **4(1)**, 6 (2019).

[59] Ghosh, S., Brückner, F., Nikitin, A., Grinenko, V., Elender, M., Luetkens, H., Klauss, H.-H., and Hicks, C. W. Piezoelectric-driven uniaxial pressure cell for muon spin relaxation and neutron scattering experiments. *Rev. Sci. Inst.* **91**, 103902 (2020).

[60] Maisuradze, A., Khasanov, R., Shengelaya, A., and Keller, H. Comparison of different methods for analyzing μSR line shapes in the vortex state of type-II superconductors. *J. Phys.: Condens. Matter* **21**, 075701 (2009).

[61] Suter, A. and Wojek, B. M. Musrfit: A Free Platform-Independent Framework for μSR Data Analysis. *Phys. Procedia* **30**, 69-73 (2012).

[62] Clawson, C. W., Crowe, K. M., Rosenblum, S. S., Kohn, S. E., Huang, C. Y., Smith, J. L., and Brewer, J. H. Low-Temperature Mobility of Positive Muons in Copper. *Phys. Rev. Lett.* **51**, 114–117 (1983).

[63] Brandt, E. H. Properties of the ideal Ginzburg-Landau vortex lattice. *Phys. Rev. B* **68**, 054506 (2003).

[64] Grinenko, V., Sarkar, R., Materne, P., Kamusella, S., Yamamshita, A., Takano, Y., Sun, Y., Tamegai, T., Efremov, D. V., Drechsler, S.-L., Orain, J.-C., Goko, T., Luetkens, H., and

Klauss, H.-H. Low-temperature breakdown of antiferromagnetic quantum critical behavior in FeSe *Phys. Rev. B* **97**, 201102(R) (2018).

FIGURE 1. **Hypothesis and setup.** **(a)** Schematic mean-field stress-temperature phase diagram for chiral superconductivity in clean Sr_2RuO_4, in the $\sigma \to 0$ limit where only σ-linear components of the stress dependence are relevant. "Δ_x" stands for either p_x or d_{xz}. **(b)** Schematic of the sample setup for μSR. The chamfers, used for Samples E and F, are intended to smooth the stress profile and reduce the maximum shear stress in the sample. Concentric coils behind the sample are used for in situ measurement of T_c.

FIGURE 2. **Results on unstressed $\mathbf{Sr_2RuO_4}$.** **(a)** Example of zero-field μSR asymmetry time spectra $A(t)$ of Sample B above and below T_{TRSB}. **(b - d)** Comparison of the temperature dependence of the zero field muon relaxation rate $\lambda(T)$ (left scale) and heat capacity data (right scale) for Samples A, B and C, all under zero stress. To determine T_{TRSB}, $\lambda(T)$ is fit with a quadratic form: $\lambda(T) = \lambda_0 + a[1-(T/T_{\mathrm{TRSB}})^2]$ for $T < T_{\mathrm{TRSB}}$, and $\lambda(T) = \lambda_0$ for $T > T_{\mathrm{TRSB}}$. The displayed error bars correspond to one standard deviation from the χ^2 fit.

FIGURE 3. **Stress-induced splitting between $\boldsymbol{T_c}$ and $\boldsymbol{T_{\mathrm{TRSB}}}$.** Left-hand panels: Zero-field μSR asymmetry $A(t)$ at a temperature above T_c, and at the lowest temperature reached at each stress. **(a–c)** Sample D at 0 GPa, -0.28 GPa and -0.43 GPa, **(d)** Sample E at -0.70 GPa, and **(e)** Sample F at -0.79 GPa. **(f–h)**: Temperature dependence of the muon spin relaxation rate λ, and in situ diamagnetic susceptibility data for sample D. The applied field for the susceptibility measurements was of the order of 10 μT. Heat capacity and transverse-field μSR data show that the samples are fully superconducting, so we identify the extrema of the susceptibility signal as $4\pi\chi = 0$ and -1 (see also Fig. ED5). The fits to $\lambda(T)$ (red lines) are explained in the text. To avoid biasing the analysis, the same temperature range, which excludes the three open points in panel (h), was used for the Sample D fits in panels (f-h). **(i–j)** λ and $4\pi\chi$ for Samples E and F. The displayed error bars correspond to one standard deviation from the χ^2 fit.

FIGURE 4. **Magnetic order.** **(a)** Zero-field asymmetry $A(t)$ at various temperatures for Sample F at -1.05 GPa. **(b)** The maximum internal field B_{max} and transverse signal fraction α as a function of temperature. The fit to B_{max} gives $T_{\mathrm{N}} = 6.86$ K. **(c)** Transverse and longitudinal relaxation rates versus temperature. Error bars, when not shown, are smaller than the symbol. **(d)** In situ diamagnetic susceptibility data. $T_{\mathrm{c}} \sim 1$ K is defined using a 50% criterion. The displayed error bars correspond to one standard deviation from the χ^2 fit.

FIGURE 5. **Experimental phase diagram.** The stress-temperature phase diagram of Sr_2RuO_4 based on the data presented here. SDW stands for spin density wave. SC denotes a single component superconducting state (d or s - wave), and TRSB SC denotes two-component superconductivity. Possible even-parity candidates are d+id, s+id, and d+ig. Data are plotted against stress, which may be converted to strain using the low-temperature Young's modulus of 160 GPa [28]. The insets illustrate the stress-induced changes in the Fermi surfaces of Sr_2RuO_4: the peak in T_{c} is approximately the stress at which the largest Fermi surface passes through a Lifshitz transition, at the Y point of the Brillouin zone [28]. The displayed error bars correspond to the 10 % and 90 % criteria of the ac-susceptibility signal change at the superconducting transition.

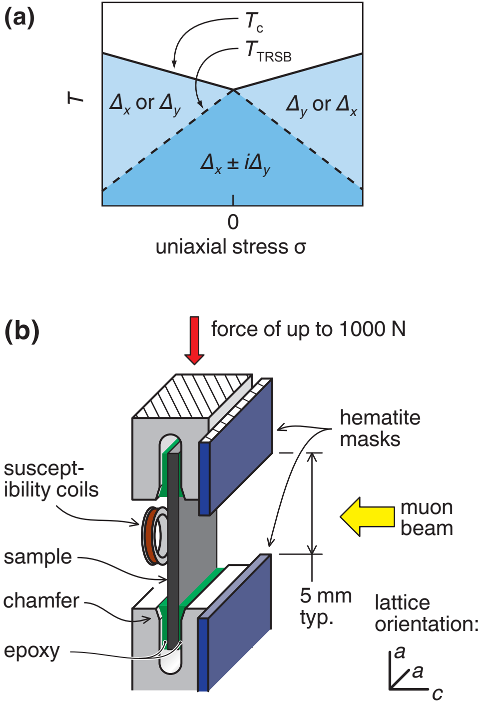
(a)
T_c
T_{TRSB}
T
Δ_x or Δ_y
Δ_y or Δ_x
$\Delta_x \pm i\Delta_y$
0
uniaxial stress σ
(b)
force of up to 1000 N
hematite masks
suscept-ibility coils
muon beam
sample
chamfer
epoxy
5 mm typ.
lattice orientation:
a
a
c

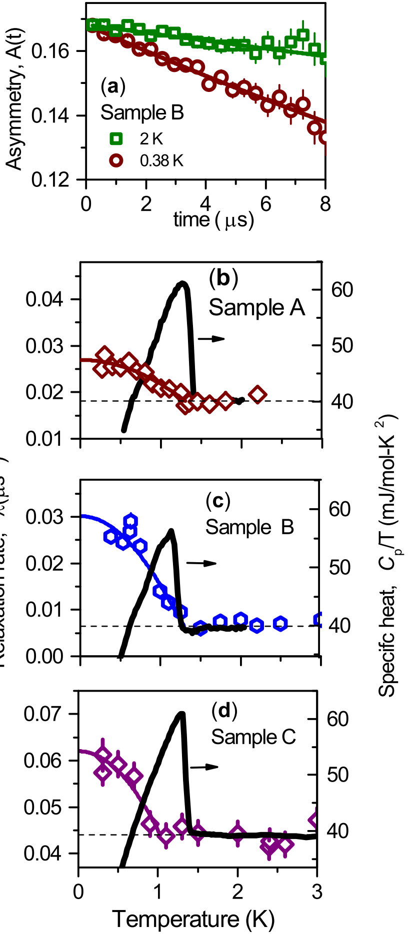

Asymmetry, A(t)
0.16
0.14
0.12
(a)
Sample B
2 K
0.38 K
0 2 4 6 8
time (μs)
(b)
Sample A
0.04
0.03
0.02
0.01
60
50
40
(c)
Sample B
0.03
0.02
0.01
0.00
Relaxation rate, λ(μs⁻¹)
Specifc heat, Cp/T (mJ/mol-K²)
(d)
Sample C
0.07
0.06
0.05
0.04
0 1 2 3
Temperature (K)

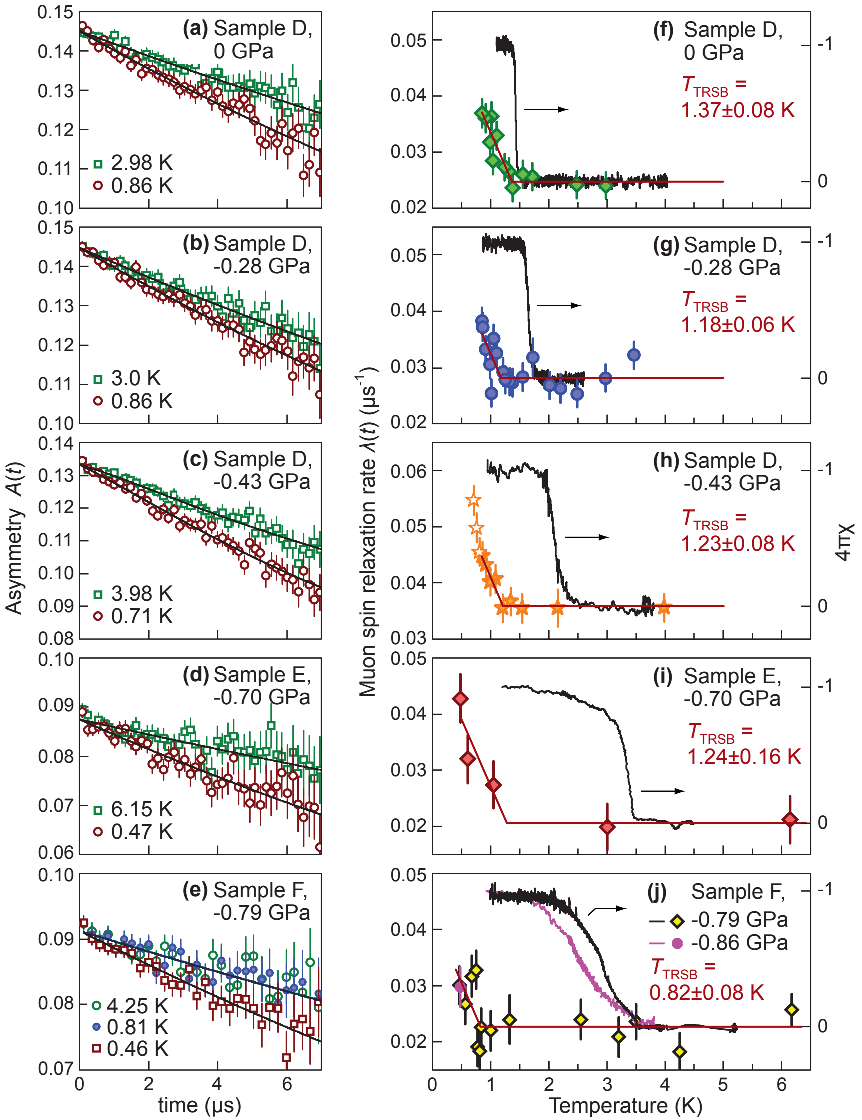

(a) Sample D, 0 GPa
2.98 K
0.86 K
(b) Sample D, -0.28 GPa
3.0 K
0.86 K
(c) Sample D, -0.43 GPa
3.98 K
0.71 K
(d) Sample E, -0.70 GPa
6.15 K
0.47 K
(e) Sample F, -0.79 GPa
4.25 K
0.81 K
0.46 K
Asymmetry A(t)
time (μs)
(f) Sample D, 0 GPa
T_TRSB = 1.37±0.08 K
(g) Sample D, -0.28 GPa
T_TRSB = 1.18±0.06 K
(h) Sample D, -0.43 GPa
T_TRSB = 1.23±0.08 K
(i) Sample E, -0.70 GPa
T_TRSB = 1.24±0.16 K
(j) Sample F,
-0.79 GPa
-0.86 GPa
T_TRSB = 0.82±0.08 K
Muon spin relaxation rate λ(t) (μs^-1)
4πχ
Temperature (K)

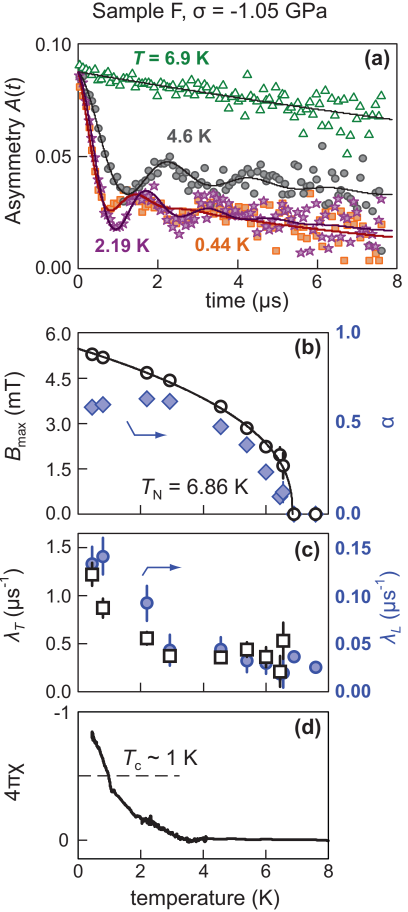

Sample F, σ = -1.05 GPa
(a)
T = 6.9 K
4.6 K
2.19 K
0.44 K
Asymmetry A(t)
time (μs)
(b)
B_max (mT)
α
T_N = 6.86 K
(c)
λ_T (μs^-1)
λ_L (μs^-1)
(d)
4πχ
T_c ~ 1 K
temperature (K)

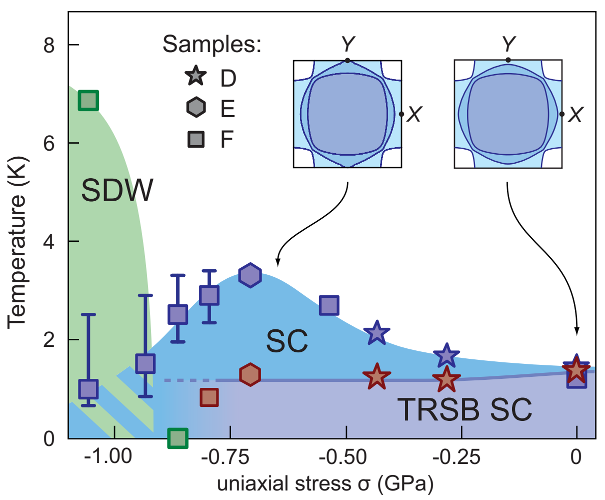

Samples:
D
E
F
Y
X
Y
X
SDW
SC
TRSB SC
Temperature (K)
8
6
4
2
0
-1.00
-0.75
-0.50
-0.25
0
uniaxial stress σ (GPa)

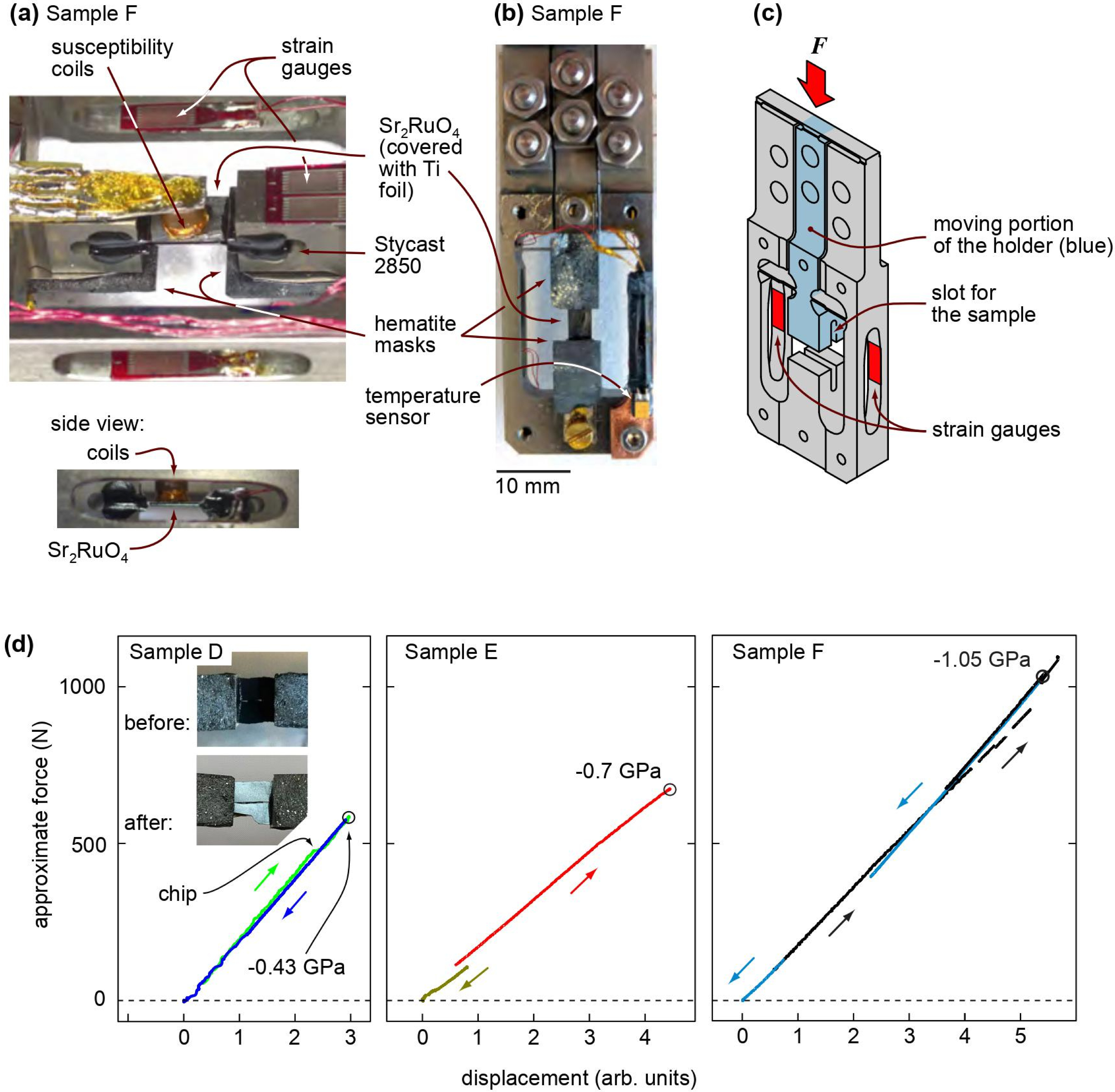

(a) Sample F
susceptibility coils
strain gauges
Sr$_2$RuO$_4$ (covered with Ti foil)
Stycast 2850
hematite masks
side view:
coils
Sr$_2$RuO$_4$
(b) Sample F
temperature sensor
10 mm
(c)
F
moving portion of the holder (blue)
slot for the sample
strain gauges
(d)
Sample D
before:
after:
chip
-0.43 GPa
Sample E
-0.7 GPa
Sample F
-1.05 GPa
approximate force (N)
displacement (arb. units)
0
500
1000
0
1
2
3
4
5

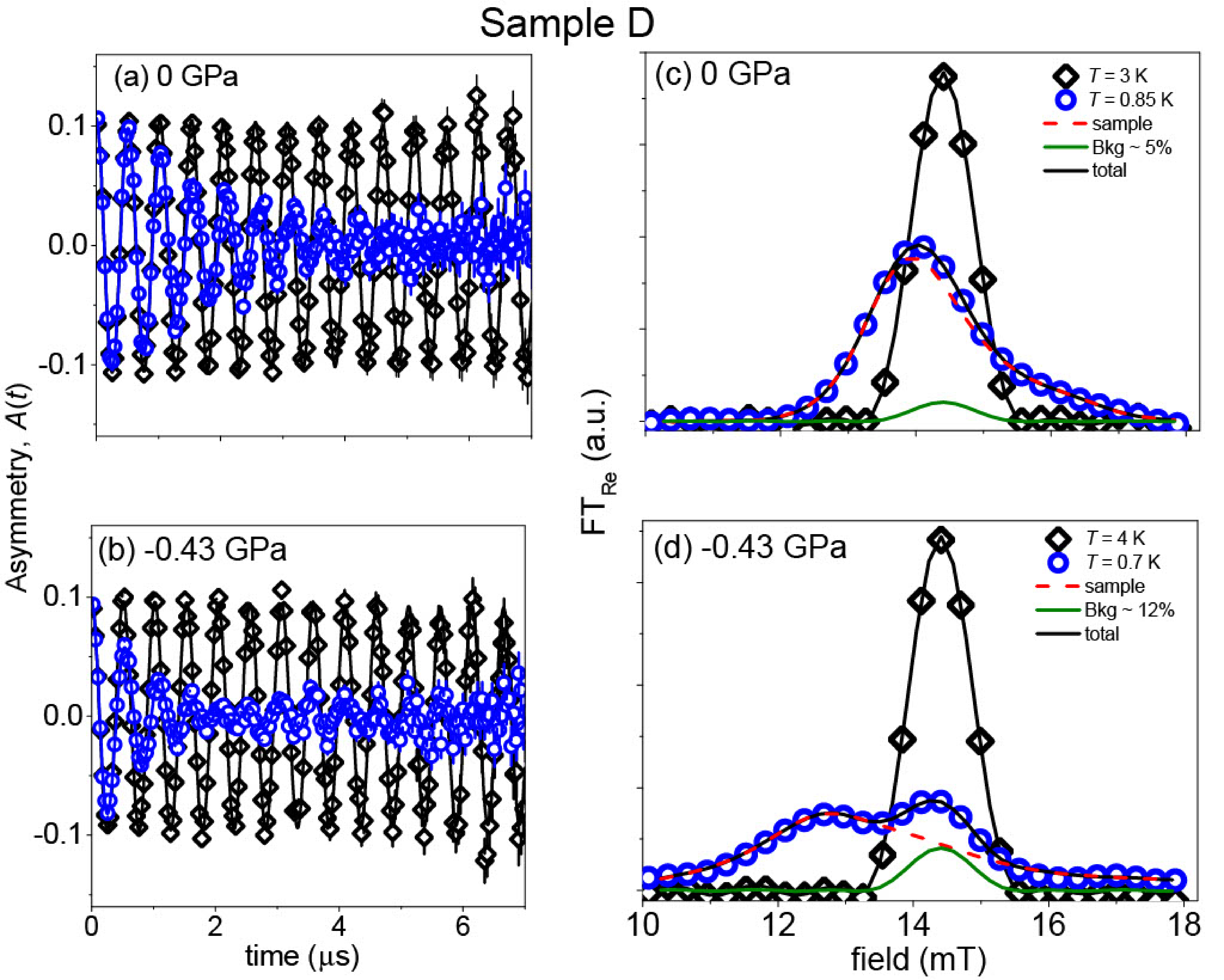

Sample D
(a) 0 GPa
(b) -0.43 GPa
Asymmetry, A(t)
time (μs)
(c) 0 GPa
T = 3 K
T = 0.85 K
sample
Bkg ~ 5%
total
(d) -0.43 GPa
T = 4 K
T = 0.7 K
sample
Bkg ~ 12%
total
FT_Re (a.u.)
field (mT)

Sample D at -0.43 GPa

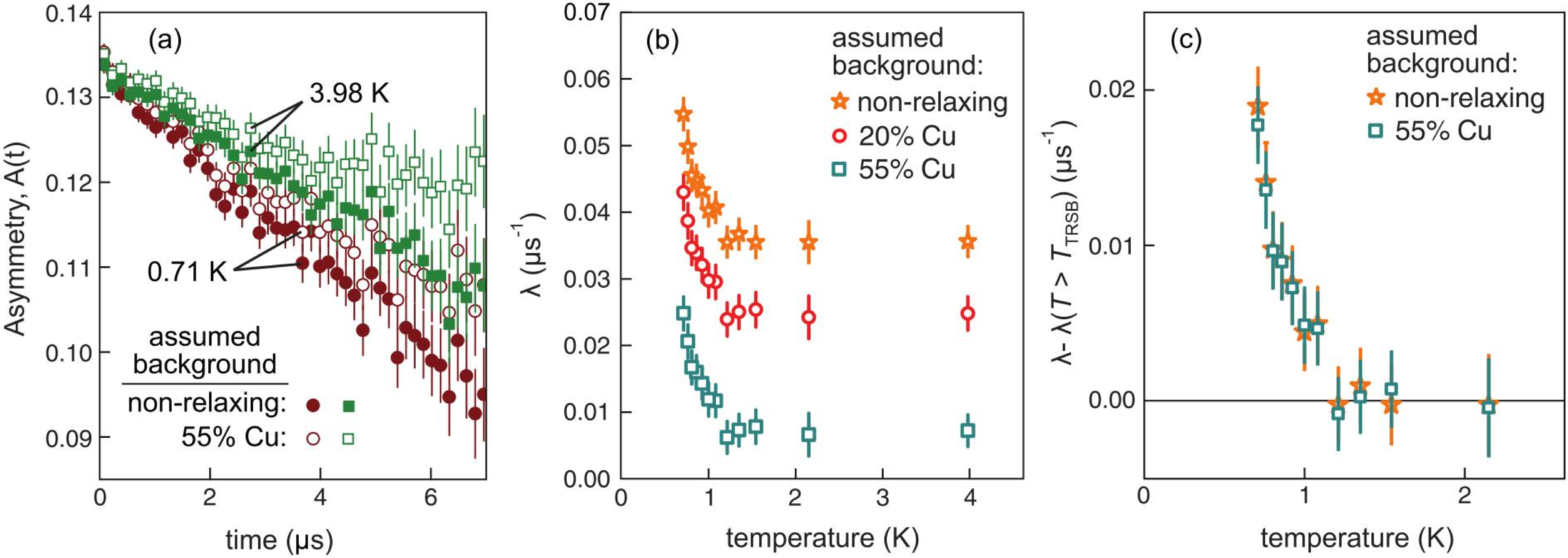

Comparison of Samples A and A2 at 0 GPa:

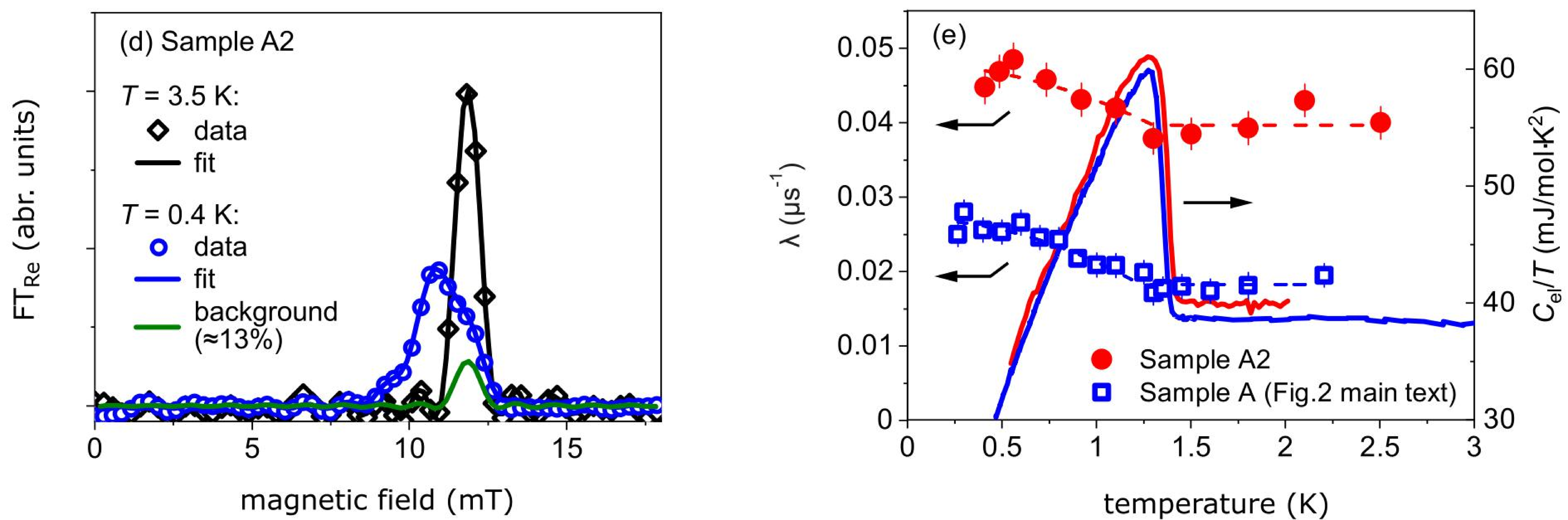

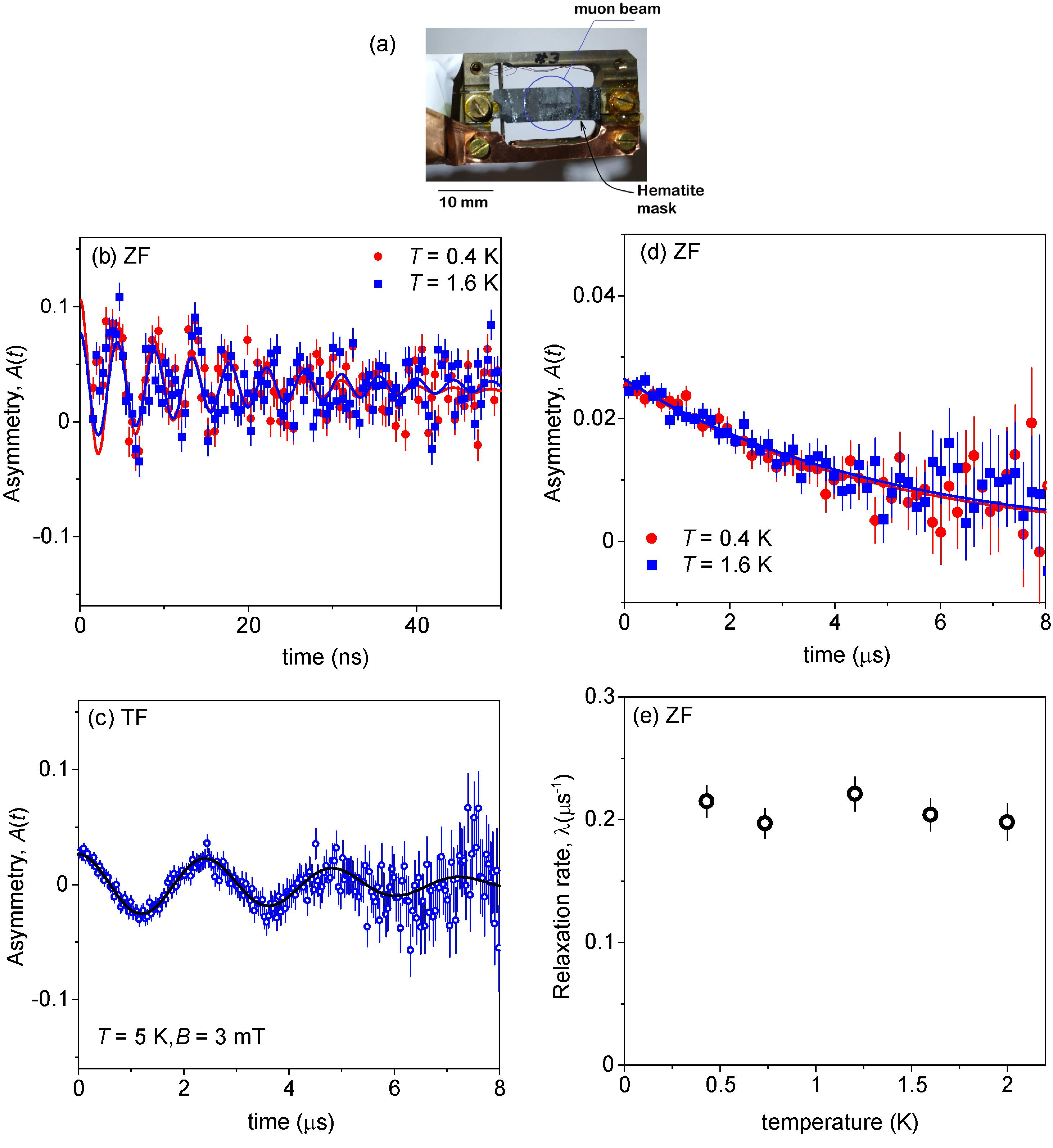

(a)
muon beam
10 mm
Hematite mask
(b) ZF
T = 0.4 K
T = 1.6 K
Asymmetry, A(t)
time (ns)
(c) TF
T = 5 K, B = 3 mT
time (μs)
(d) ZF
(e) ZF
Relaxation rate, λ(μs^-1)
temperature (K)

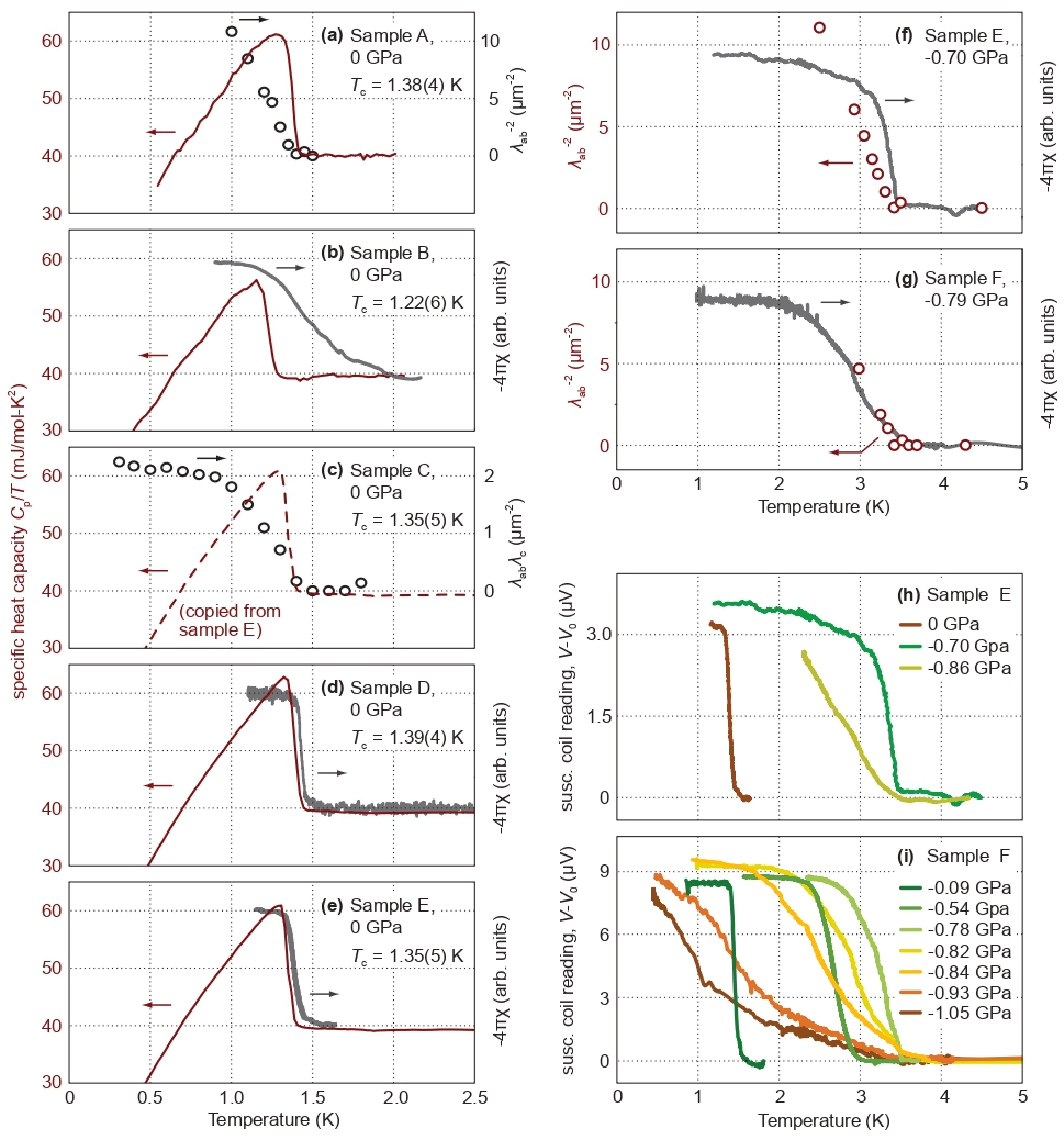

(a) Sample A, 0 GPa
T_c = 1.38(4) K
(b) Sample B, 0 GPa
T_c = 1.22(6) K
(c) Sample C, 0 GPa
T_c = 1.35(5) K
(copied from sample E)
(d) Sample D, 0 GPa
T_c = 1.39(4) K
(e) Sample E, 0 GPa
T_c = 1.35(5) K
specific heat capacity C_p/T (mJ/mol-K^2)
λ_{ab}^{-2} (μm^{-2})
$\lambda_{ab}\lambda_c$ (μm^{-2})
-4πχ (arb. units)
Temperature (K)
(f) Sample E, -0.70 GPa
(g) Sample F, -0.79 GPa
(h) Sample E
0 GPa
-0.70 Gpa
-0.86 GPa
(i) Sample F
-0.09 GPa
-0.54 Gpa
-0.78 GPa
-0.82 GPa
-0.84 GPa
-0.93 GPa
-1.05 GPa
susc. coil reading, V-V_0 (μV)

Sample F, σ = 1.05 GPa, T = 2.9 K
0.10
0.08
0.06
0.04
0.02
0.00
Asymmetry A(t)
0
2
4
6
time (μs)
Bessel
Cos
0.10
0.05
0.00
Asymmetry A(t)
0.0
0.2
0.4
0.6
time (μs)
χ² = 1.018
χ² = 1.10

(a)
$K_{B||ab}$ (ppm)
-220
-222
-224
-226
0
1
2
3
4
temperature (K)
Fuorier power (abr. units)
Sr_2RuO_4
Ag-holder
T = 0.12 K
8.000
8.005
8.010
field (T)
(b)
Sr_2RuO_4
Ag-holder
Relaxation rate, λ (μs^{-1})
0.08
0.06
0.04
0.02
0.00
0
1
2
3
4
temperature (K)